

# Revisiting the Thermal Transition of $\beta$ -Form Polyamide-6: Evolution of Structure and Morphology in Uniaxially Stretched Films

Jia-Ru Xu,<sup>†</sup> Xiang-Kui Ren,<sup>‡</sup> Tao Yang,<sup>†</sup> Xu-Qiang Jiang,<sup>†</sup> Wen-Ying Chang,<sup>†</sup> Shuang Yang,<sup>†</sup> Alexander Stroeks,<sup>\*,§</sup> and Er-Qiang Chen<sup>\*,†</sup>

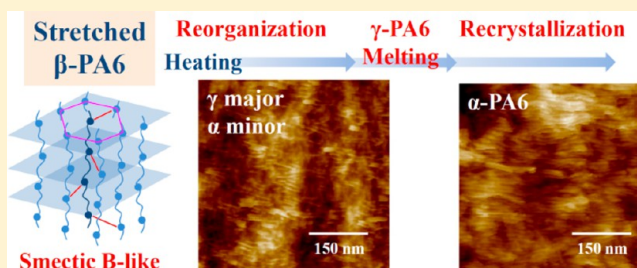
<sup>†</sup>Beijing National Laboratory for Molecular Sciences, Department of Polymer Science and Engineering and the Key Laboratory of Polymer Chemistry and Physics of Ministry of Education, Center for Soft Matter Science and Engineering, College of Chemistry and Molecular Engineering, Peking University, Beijing 100871, China

<sup>‡</sup>School of Chemical Engineering and Technology, Tianjin University, Tianjin 300350, China

<sup>§</sup>DSM Materials Science Center, DSM Ahead, P.O. Box 1066, 6160 BB Geleen, The Netherlands

## Supporting Information

**ABSTRACT:** Structure and morphology evolution of the uniaxially stretched polyamide-6 (PA6) film with the  $\beta$ -form upon heating were investigated mainly by synchrotron two-dimensional (2D) wide-angle X-ray diffraction and small-angle X-ray scattering. For comparison, thermal transitions of the oriented PA6 samples with the  $\alpha$ - and  $\gamma$ -form were also monitored, which undergo “incomplete Brill transition” and direct melting, respectively. Using the results of oriented  $\alpha$ - and  $\gamma$ -PA6 as the references, we confirm that the stretched  $\beta$ -PA6 is mesomorphic, which can be viewed as a solid mesophase with smectic B-like parameters. We identify that upon heating the stretched  $\beta$ -PA6 reorganizes dominantly into  $\gamma$ -form crystal with the chain orientation unchanged, accompanied by the formation of a little amount of  $\alpha$ -PA6 crystallites. Further heating to above the melting temperature of  $\gamma$ -PA6, the  $\alpha$ -PA6 crystals grow through a recrystallization process. The lamellae resulting from reorganization exhibit a distribution of orientations, and the  $\alpha$ -PA6 lamellae formed at high temperatures have the lamellar basal surface normal parallel to the stretched direction. We consider that the abundant hydrogen bonds in the stretched  $\beta$ -PA6 film construct a network, providing the confinement effect to reduce the chain mobility and thus favor the formation of  $\gamma$ -form. The lamellae with the basal surface normal tilted relative to the stretched direction can also be attributed to the hydrogen-bonded network of oriented chains.



## INTRODUCTION

As one of the most widely used engineering plastics, polycaprolactam (nylon-6 or PA6) has exhibited excellent properties in many areas such as automotive, textile, and packaging applications.<sup>1–3</sup> Since the amide linkage and methylene sequence are alternatively placed along the chain, hydrogen-bonding interaction between adjacent PA6 chains plays the critical role to determine how the chains pack together, the same as that happened in other nylons.<sup>4–7</sup> Variation of the interchain hydrogen bonds causes the complex polymorphism of PA6. In the  $\alpha$ -form of PA6 crystals, the hydrogen bonds are formed between antiparallel chains which adopt a fully extended zigzag chain conformation. The  $\alpha$ -form is monoclinic with the unit cell parameters  $a = 9.56$  Å,  $b$  (chain axis) = 17.24 Å,  $c = 8.01$  Å, and  $\beta = 67.5^\circ$ .<sup>8</sup> The  $\gamma$ -form of PA6, also monoclinic, is metastable compared to the  $\alpha$ -form.<sup>9–12</sup> Detailed X-ray analysis reveals that in the  $\gamma$ -form the hydrogen bonds are formed between parallel chains. The amide groups along the chains twist approximately  $60^\circ$  out of the methylene zigzag plane, making the  $b$ -axis slightly shorter than that in  $\alpha$ -form. The monoclinic  $\gamma$ -form possesses the unit cell parameters

$a = 9.33$  Å,  $b$  (chain axis) = 16.88 Å,  $c = 4.78$  Å, and  $\beta = 121^\circ$ .<sup>13</sup> Because the  $d$ -spacings of (200) and (001) are almost identical, the  $\gamma$ -form is also referred to as pseudo-hexagonal structure. The growth of the  $\alpha$ - and  $\gamma$ -form of PA6 is greatly dependent on the crystallization condition.<sup>14,15</sup> Isothermal crystallization or slow cooling results in  $\alpha$ -PA6 crystals.  $\gamma$ -PA6 is usually formed through rapid crystallization during fast cooling, drawing, or spinning. The pure  $\gamma$ -PA6 can also be obtained from  $\alpha$ -form by KI/I<sub>2</sub> treatment.<sup>16,17</sup>

For PA6, besides the  $\alpha$ - and  $\gamma$ -form, the so-called  $\beta$ -form is also very important in terms of processing and application, which can be obtained by quenching PA6 from the molten state.<sup>15,18,19</sup> Fourier transform infrared spectroscopy (FTIR) results indicate that the chains in  $\beta$ -form possess the conformation largely similar to that in amorphous.<sup>20</sup> On the other hand, the wide-angle X-ray diffraction (WAXD) pattern of  $\beta$ -PA6 looks somewhat like that of the  $\gamma$ -form. However, as

Received: August 24, 2017

Revised: November 14, 2017

Published: December 27, 2017

shown by the melt spun fiber, typically, the  $\beta$ -form only presents the diffractions on equator and meridian (chain axis), with the former corresponding to  $\sim 0.42$  nm and the latter fairly the length of one repeating unit. These outcomes indicate that the  $\beta$ -form is less ordered than the  $\gamma$ -form and, most likely, a mesophase. Ziabicki has first proposed that PA6 chains in the  $\beta$ -form pack parallel to each other, forming a pseudo-hexagonal structure with the hydrogen bonds randomly distributed around the chain axis.<sup>18</sup> Recently, a refined model by Auriemma et al. considers that the  $\beta$ -form is made up of small mesomorphic aggregates of chains packed in a hexagonal lattice and the hydrogen bonds can be along  $[100]$ ,  $[010]$ , and  $[\bar{1}\bar{1}0]$  directions (with  $c$ -axis the chain axis),<sup>21</sup> wherein the chains can form almost 100% hydrogen bonds. There are also some other chain packing models suggested. For example, Stepaniak et al. reported that some PA6 fibers produced by a fast spinning route, which exhibited the typical  $\beta$ -form diffraction, could be easily converted to  $\alpha$ -form. To account for this, they have postulated that in the fiber there is a pleated  $\alpha$  structure with hydrogen bonds joined by antiparallel chains.<sup>22</sup> Murthy observed that stretching the  $\gamma$ -PA6 fibers could result in a metastable crystal, of which the diffraction shared some features of the  $\beta$ -PA6. As it would transform into either  $\alpha$ - or  $\gamma$ -form under specific thermomechanical treatments, an intermediate structure of “random sheets”, wherein the hydrogen bonds formed between both antiparallel and parallel chains, is suggested.<sup>23</sup> It is noticed that not only the chain packing but also the transition of  $\beta$ -PA6 remains controversial. Thermodynamically, the less stable  $\beta$ -PA6 always has the tendency to transform into the  $\alpha$ - and/or  $\gamma$ -form. While many works reported that the  $\beta$ -PA6 could transform to  $\alpha$ -form directly,<sup>20,22</sup> it is also described that the  $\beta$ -PA6 can relax to a mixture of  $\alpha$ - and  $\gamma$ -form.<sup>24</sup> Very recently, Pepin et al. followed the structure evolution of unoriented  $\beta$ -PA6 upon heating and subsequent cooling using one-dimensional (1D) WAXD.<sup>25</sup> They conclude that the unoriented  $\beta$ -PA6 will reorganize into a high-temperature pseudo-hexagonal phase ( $\beta'$ -form) upon heating, and the observed  $\alpha$ -PA6 at room temperature resulted from the cooling of the  $\beta'$ -form.

It can be inferred from the literature that the mesomorphic  $\beta$ -PA6 may have the degree of order sensitive to the processing conditions, owing to the dynamic nature of interchain hydrogen-bonding interaction. The sample variations due to different fabrication conditions may bring about different observations and thus the different opinions on  $\beta$ -PA6. Here, instead of using the unoriented sample, we chose the uniaxially stretched  $\beta$ -PA6 film as the model system, of which the mesophase structure can be clearly identified. To investigate the structure and transition of the crystalline polymers with a complex polymorphism, such as nylons, the oriented samples have their own advantages.<sup>26</sup> Given that the oriented samples can present diffractions/scatterings in two dimensions (2D), a clear discrimination among different phases can be achieved and, moreover, the transformation from one phase to the other can be well resolved.

In this paper, we mainly employed temperature-dependent synchrotron 2D WAXD to monitor the thermal transition of the stretched  $\beta$ -PA6 film. Furthermore, thermal 2D small-angle X-ray scattering (SAXS) was carried out to follow the evolution of lamellar morphology in the  $\beta$ -PA6, which was not well studied before. For comparison, the highly oriented  $\alpha$ - and  $\gamma$ -PA6 were also investigated. On the basis of the experimental results, we consider that the stretched  $\beta$ -PA6 can be viewed as a

solid mesophase with smectic B (SmB)-like structure, wherein there is a hydrogen-bonded network of the oriented chains. Upon heating, the chain orientation is well maintained. First, the  $\beta$ -PA6 dominantly reorganizes into the  $\gamma$ -PA6 lamellae, accompanied by the formation of a little amount of  $\alpha$ -PA6 crystallites. The  $\gamma$ -PA6 lamellae with a distribution of orientation will be melted with increasing temperature, followed by a fast crystallization of the  $\alpha$ -PA6 lamellae with their basal surface normal parallel to the stretching direction. In this work, we also determine the monoclinic cell parameters of  $\alpha$ -form changing with temperature. The observation suggests that during heating the  $\alpha$ -PA6 crystals can undergo an “incomplete Brill transition”, which was proposed by Murthy for the unoriented PA6 but not affirmed before.<sup>27</sup>

## ■ EXPERIMENTAL SECTION

**Materials and Sample Preparation.** The uniaxially stretched  $\beta$ -PA6 films (Akulon F136 C1) provided by DSM (Geleen, the Netherlands), having a molecular weight of  $\sim 20$  kg/mol, were prepared by quenching the cast PA6 films at a chill roll of 20 °C, followed by uniaxial stretching at 57 °C to a draw ratio of 4. Directly after stretching, the films were packed in alumina bags to prevent moisture uptake.

Using the stretched  $\beta$ -PA6 film as the precursor, we prepared the  $\alpha$ - and  $\gamma$ -PA6 film with high orientation. To obtain the  $\alpha$ -PA6, the  $\beta$ -PA6 film was placed on a homemade hot stage which was in a sealed steel jar fulfilled with dry nitrogen gas. Without any mechanical constraint, the film was heated from room temperature to 219 °C. After subjected to isothermal annealing for 30 min, the film was cooled back to room temperature. The annealing temperature was controlled to better than  $\pm 1$  °C. The  $\gamma$ -PA6 film was prepared using KI/I<sub>2</sub> treatment.<sup>16,17</sup> The  $\beta$ -PA6 film was soaked in a 0.2 M iodine solution with an KI/I<sub>2</sub> ratio of 1/2 for a week at room temperature. Afterward, the film was transferred to a 0.5 M sodium thiosulfate solution for a week to remove the absorbed iodine, followed by washing in deionized water for 2 days. Both the  $\alpha$ - and  $\gamma$ -PA6 films were dried thoroughly and stored in vacuum before usage.

**Instrument and Experiments.** A TA Q100 DSC was used to examine the thermal behaviors of PA6. The oriented film samples were cut into small pieces and encapsulated in hermetically sealed aluminum pans, with a typical sample weight of  $\sim 3$  mg. A heating rate of 10 °C/min was used. The temperature and heat of fusion were calibrated using standard materials.

2D WAXD and SAXS experiments of PA6 were performed at the Beamline 1W2A of the Beijing Synchrotron Radiation Facility (BSRF). The X-ray wavelength ( $\lambda$ ) was 1.2398 Å. For the WAXD and SAXS measurement, the sample-to-detector (Mar165 detector) distances were 162 and 1950 mm, respectively. A Linkman THMSE600 hot stage was mounted on the sample stage of the beamline to control the sample temperature. No mechanical fixation was applied for the films. During the measurement, the sample was heated up to 230 °C step by step under the protection of dry nitrogen gas. At each selected temperature, after the sample was equilibrated for 180 s, the 2D WAXD or SAXS data were acquired in situ for 300 s. The diffraction/scattering peak was calibrated by silver behenate. The background scattering was recorded and subtracted from the sample patterns. Some WAXD experiments were also performed on a modified Xeuss system (Xenocs SA, France), with a multilayer focused Cu K $\alpha$  radiation as the X-ray source (Genix3D Cu ULD). The distance between sample and detector was 203.15 mm. Each 2D WAXD pattern was collected for 30 min using a semiconductor detector (Pilatus 100 K, DECTRIS, Swiss). The equatorial and/or meridional scans were obtained by integrating the diffraction/scattering intensity in a small sector around azimuth. The crystallinity was estimated based on the 1D curves of intensity ( $I$ ) vs  $2\theta$  obtained from the full screen integration of the 2D WAXD patterns, from which amorphous scatter and crystalline diffraction can be separated. In order to let readers to compare easily the data to that reported in literatures which were

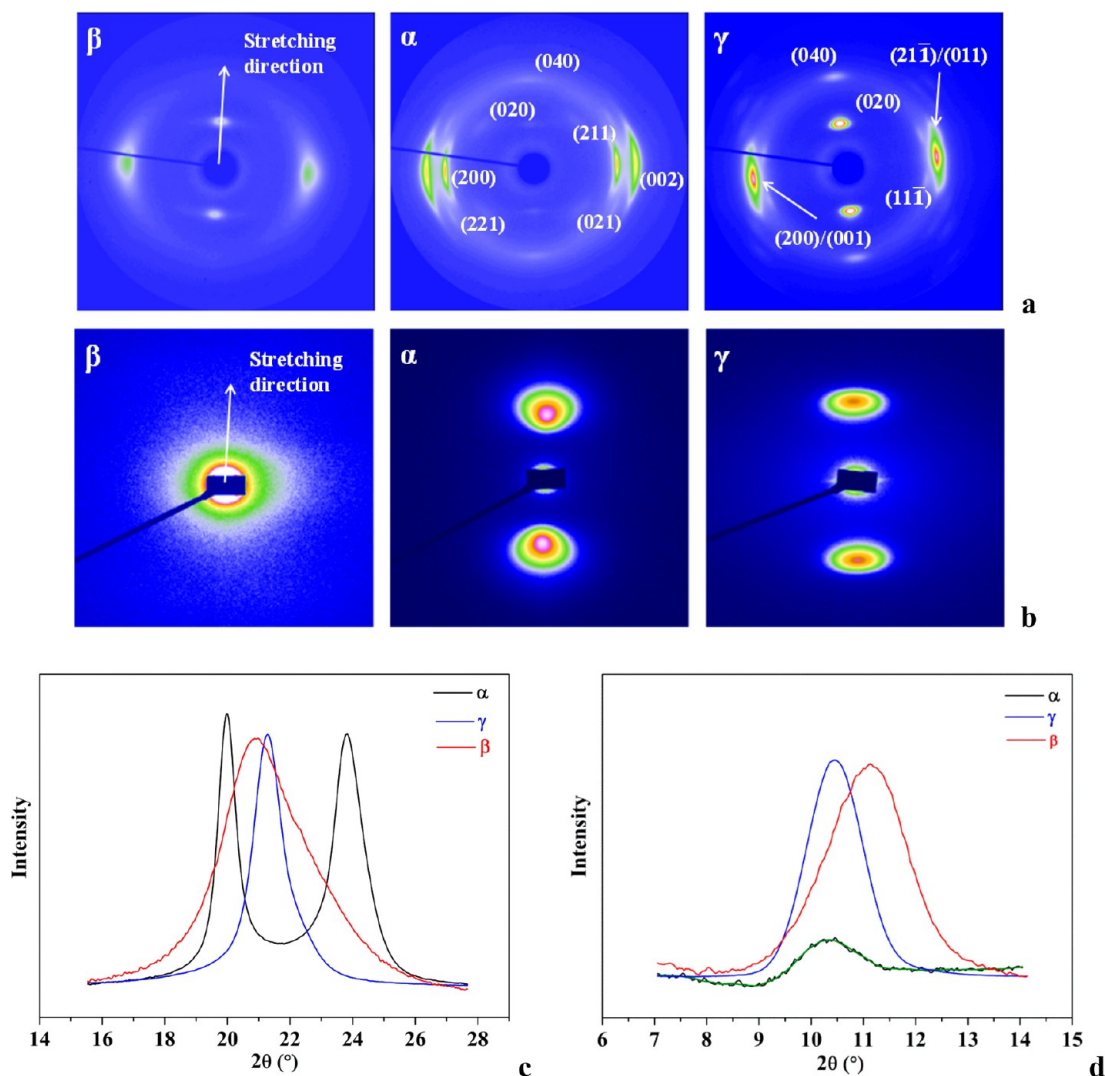


**Figure 1.** (a) 2D WAXD and (b) SAXS patterns of the oriented  $\beta$ -,  $\alpha$ -, and  $\gamma$ -PA6 films recorded at room temperature. (c, d) 1D intensity scans along equator (c) and meridian (d) obtained from the corresponding 2D WAXD patterns in (a). The stretched direction of the films is shown by the arrows in (a) and (b).

usually measured with the Cu  $K\alpha$  radiation, all the 1D WAXD curves in this paper are plotted with the  $2\theta$  corresponds to the  $\lambda$  of 0.1542 nm.

To illustrate the lamellar morphology of the PA6 film after high temperature annealing, we performed atomic force microscopy using Dimension Icon atomic force microscopy (AFM, Bruker Nano) at room temperature. PeakForce tapping mode was applied in the experiment using SCANASYST-AIR probes (tip radius:  $\sim 2$  nm; spring constant:  $\sim 0.4$  N/m; frequency:  $\sim 70$  kHz).

FTIR experiments were performed using a Thermo Nicolet NEXUS 870 FTIR spectrometer with a liquid nitrogen cooled MCT detector. A Linkam THMS600 was used to control the sample temperature. The sample was heated up to 200 °C step by step. After being held at each temperature for 5 min, the FTIR spectrum was in situ recorded with a  $4\text{ cm}^{-1}$  resolution. During the experimental process, the sample was protected by dry nitrogen gas. Attenuated total reflectance (ATR)-FTIR experiment of the PA6 samples was also performed at room temperature using this equipment.

## RESULTS

**Identification of  $\beta$ -Form of Stretched PA6.** The stretched  $\beta$ -PA6 film was first characterized using 2D WAXD and SAXS at room temperature. For comparison, the same X-ray experiments were also carried out on the  $\alpha$ - and  $\gamma$ -PA6

samples, which were prepared by 219 °C annealing and KI/I<sub>2</sub> treatment, respectively, using the stretched  $\beta$ -PA6 film as the precursor.

Figure 1a presents the 2D WAXD patterns of the three orientated PA6 samples. For the  $\alpha$ -PA6 film, all the diffractions, including those locating in the quadrants, can be well indexed using the monoclinic structures reported.<sup>8</sup> The same can be said for the  $\gamma$ -PA6 samples we prepared.<sup>13</sup> Note that the KI/I<sub>2</sub> treatment is usually used to transform the  $\alpha$ - to  $\gamma$ -form. Our experiment demonstrates that this method also works for the oriented  $\beta$ -AP6. With the stretching direction (i.e., the chain direction) along the meridian, the  $(h0l)$  diffractions of  $\alpha$ - and  $\gamma$ -PA6 appear on the equator. The  $(200)$  and  $(002)$  diffraction of  $\alpha$ -PA6 locate at  $2\theta$  of 20.1° and 23.8°, respectively. For  $\gamma$ -PA6, the single strong diffraction at  $2\theta$  of 21.3° on the equator, the characteristic of pseudohexagonal structure, is attributed to the diffractions of  $(200)$  and  $(001)$  superimposed together. On the meridian,  $\alpha$ -PA6 exhibits the weak  $(020)$  diffraction, but for  $\gamma$ -PA6, the diffraction is strong. In Figure 1b, the 2D SAXS patterns of the orientated  $\alpha$ - and  $\gamma$ -PA6 show clearly the small angle scattering peaks concentrated on the meridian (i.e., the stretching direction) at around  $q$  of  $0.6\text{ nm}^{-1}$  ( $q = 4\pi \sin \theta/\lambda$ ,

with  $2\theta$  the scattering angle), indicating that the lamellae have the basal surface normal parallel to the chain axis. The 2D WAXD and SAXS results of  $\alpha$ - and  $\gamma$ -PA6 samples indicate that the PA6 chain orientation induced by stretching is well retained during the high-temperature annealing at 219 °C and/or the KI/I<sub>2</sub> treatment.

The 2D WAXD pattern of the oriented  $\beta$ -PA6 shown in Figure 1a looks similar to that of  $\gamma$ -PA6, wherein strong diffractions can be seen on both the equator and the meridian. The quantitative comparisons between the  $\beta$ - and  $\gamma$ -PA6 for the equatorial and meridional diffraction are shown in Figures 1c and 1d, respectively, wherein the data of the  $\alpha$ -PA6 is also included. As shown Figure 1c, while completely different from the double-peaked diffraction of  $\alpha$ -PA6, the equatorial peak of  $\beta$ -PA6 is much wider and locates at a slightly lower  $2\theta$  angle in comparison with that of  $\gamma$ -PA6. The peak position corresponds to 0.43 nm, which is very close to that of (100) diffraction reported for  $\beta$ -form.<sup>21</sup> The meridional diffraction of  $\beta$ -PA6 is also broader (Figure 1d). It is known that  $\gamma$ -PA6 has the (020) diffraction at a little larger  $2\theta$  angle than  $\alpha$ -PA6 because of the twisted amide groups along the chain. The meridional diffraction of the  $\beta$ -PA6 peaks at an even larger  $2\theta$  angle. This reflects that the oriented PA6 chains in the  $\beta$ -form possess more disordered conformation. It is important to point out that the  $\beta$ -PA6 has no diffractions appearing in the quadrants, suggesting much lower ordering in comparison with the  $\gamma$ -PA6. Moreover, from the 2D SAXS pattern of  $\beta$ -PA6 (see Figure 1b) no scattering peak can be recognized, indicative of no lamellar morphology developed. As a result, the  $\beta$ -form of PA6 as a mesophase can be confirmed. We performed 2D WAXD experiment on the unstretched quenched film of PA6. Only an isotropic scattering ring at  $2\theta$  of 21.5° was observed (Figure S1 in the Supporting Information), indicating that after quenching to the glassy state the PA6 film is amorphous. Therefore, the mesomorphic  $\beta$ -PA6 studied here is induced by film stretching.

As a mesophase,  $\beta$ -PA6 shall always intend to relax into the more stable crystalline phases. Figure 2 shows the DSC heating

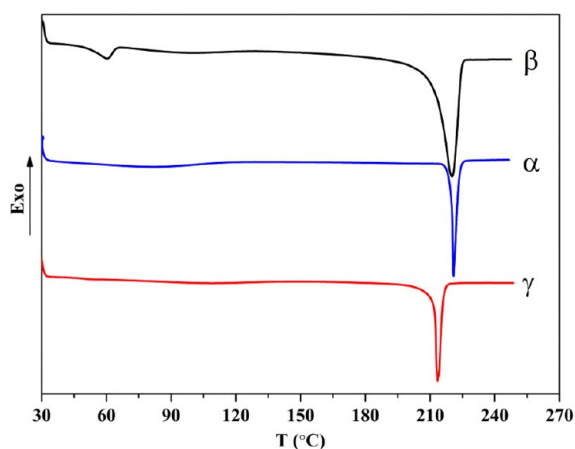


Figure 2. DSC traces of the oriented  $\beta$ -,  $\alpha$ -, and  $\gamma$ -PA6 samples recorded upon heating at 10 °C/min.

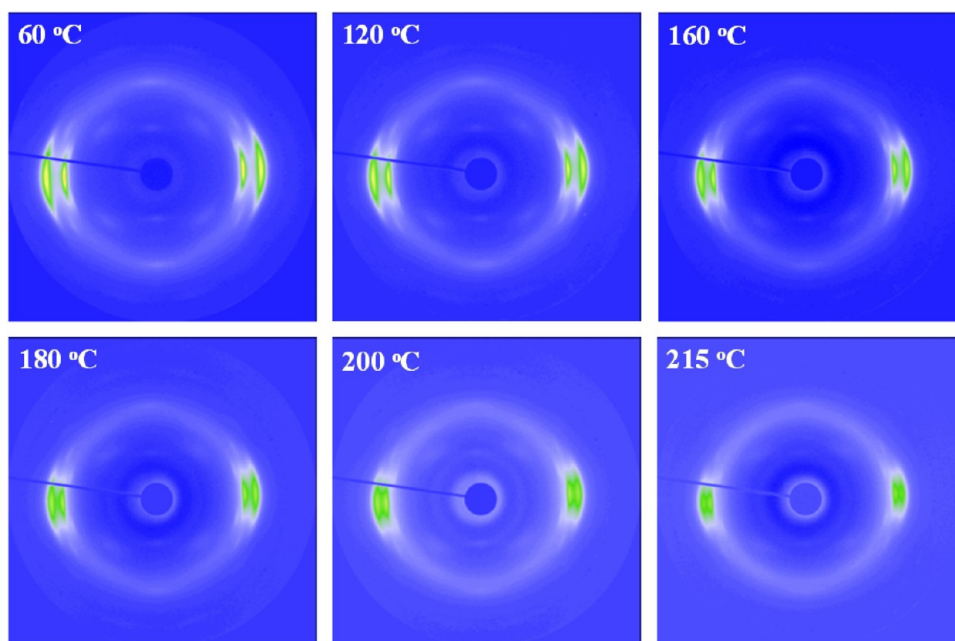
curves of the oriented  $\beta$ -,  $\alpha$ -, and  $\gamma$ -PA6 films measured at a heating rate of 10 °C/min. For  $\beta$ -PA6, a broad exothermic process appears right after the sample passed the glass transition temperature ( $T_g$ ) of  $\sim 60$  °C, evidencing an ordering process. Afterward, a relatively broad endotherm starting from  $\sim 165$  °C indicates the melting process. The melting peak

position of the  $\beta$ -PA6 sample at 220 °C is similar to that of  $\alpha$ -PA6 at 221 °C but obviously higher than that of  $\gamma$ -PA6 at 213 °C. Seemingly, the oriented  $\beta$ -PA6 mainly transform into  $\alpha$ -PA6 during the heating process. However, it is worth noting that the  $\beta$ -PA6 possesses a melting process much broader than the  $\alpha$ - and  $\gamma$ -PA6. Therefore, we cannot rule out the possibility of  $\beta$ -PA6 transforming into  $\gamma$ -PA6. The transition route of  $\beta$ -PA6 during heating will be discussed in detail later on.

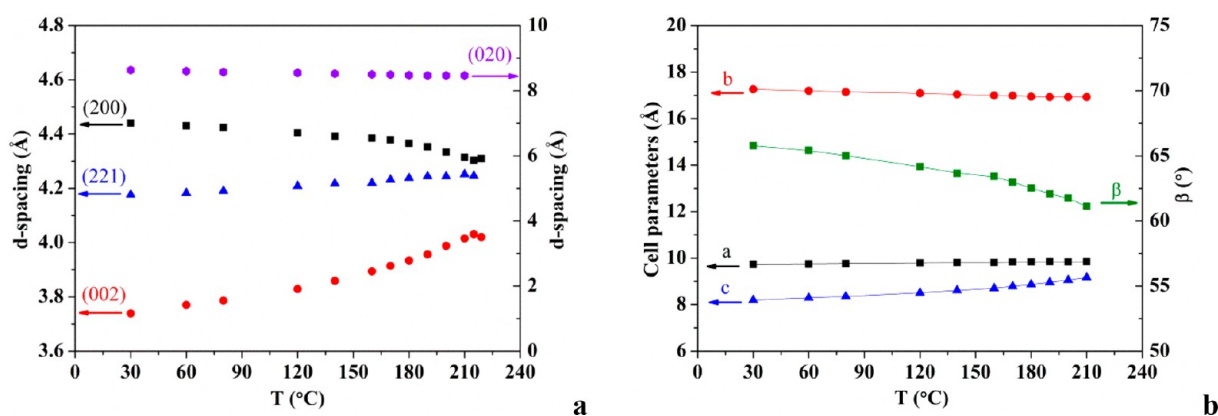
**Thermal Transition of Oriented  $\alpha$ - and  $\gamma$ -PA6.** To the end of thoroughly elucidating the thermal transition behavior of the stretched  $\beta$ -PA6, we revisited the structural changes during heating in the  $\alpha$ - and  $\gamma$ -PA6. The results can be used as the reference to identify what the crystalline structure is developed from the  $\beta$ -PA6 upon heating. In addition, the highly oriented  $\alpha$ - and  $\gamma$ -PA6 samples can provide more clearly the distinct diffractions in X-ray experiments. Therefore, although the  $\alpha$ - and  $\gamma$ -forms of PA6 have been extensively studied,<sup>27–29</sup> here the new synchrotron WAXD results can still deepen our understanding of some basic issues, such as if there is a Brill transition in  $\alpha$ -PA6.

Figure 3 shows a set of 2D WAXD patterns for  $\alpha$ -PA6 recorded at different temperatures upon heating. We observed that the chain orientation was well maintained prior to the crystal melting. With the stretching direction on the meridian, the two diffractions of (200) and (002) of  $\alpha$ -PA6 locate on the equator. They move closer to each other as the temperature rises, in consistent with that widely reported.<sup>27,28</sup> Meanwhile, the (020) diffraction on the meridian and some ( $hkl$ ) diffractions in the quadrant area can also be readily recognized. Although the diffractions move their positions more or less, they can be assigned using a same set of ( $hkl$ ) indexes. Consequently, the symmetry of chain packing of  $\alpha$ -PA6 does not change during heating. This enables us to determine the variations of unit cell parameters for the  $\alpha$ -form as functions of temperature. Without the pronounced chain orientation in the  $\alpha$ -PA6 film, this would be impossible.

Figure 4a describes the  $d$ -spacings of (200), (002), (020), and (221) of  $\alpha$ -PA6 measured at different temperatures. Accordingly, the parameters of  $a$ ,  $b$  (chain axis),  $c$ , and  $\beta$  of the monoclinic cell can be calculated (Figure 4b). The result shows that the unit cell dimensions do not significantly change with temperature, especially for the  $a$ -axis. Note that the  $a$ -axis is collinear with the hydrogen bond direction in the hydrogen-bonded sheet of the  $\alpha$ -form. The almost unchanged  $a$  parameter suggests that the hydrogen-bonded sheets exist persistently during the heating process, which should be due to the strong hydrogen-bonding interaction. The prominent change is observed for the  $\beta$  angle, which is 65.7° at 30 °C and 61.1° at 215 °C. On the other hand, the  $c$  parameter increases on heating, causing the  $d$ -spacing of (002) to increase remarkably. This indicates that the distance between the hydrogen-bonded sheets enlarges, which should be the reason for the melting of  $\alpha$ -PA6. Murthy et al. have proposed that unoriented  $\alpha$ -PA6 can possess the Brill transition, which is widely observed in nylon family.<sup>27,30–36</sup> However, for the perfect  $\alpha$ -PA6, no high-temperature pseudo-hexagonal structure is detected,<sup>27,28</sup> and thus the Brill transition is under debate. As the  $\beta$  angle we measured gets more and more close to 60°, we think that the tendency toward the Brill transition exists for  $\alpha$ -PA6. It is important to note that the hydrogen-bonded sheets survive during heating. On the basis of the studies on nylon-6,6 and nylon-10,10, which show the typical phenomenon of Brill transition, English and Tashiro have proposed that the Brill



**Figure 3.** 2D WAXD patterns of the oriented  $\alpha$ -PA6 at various temperatures recorded during the heating process. The meridian direction is parallel to the stretching direction.



**Figure 4.** (a)  $d$ -spacings of some  $(hkl)$  diffractions and (b) unit cell parameters of  $\alpha$ -PA6 as functions of temperature.

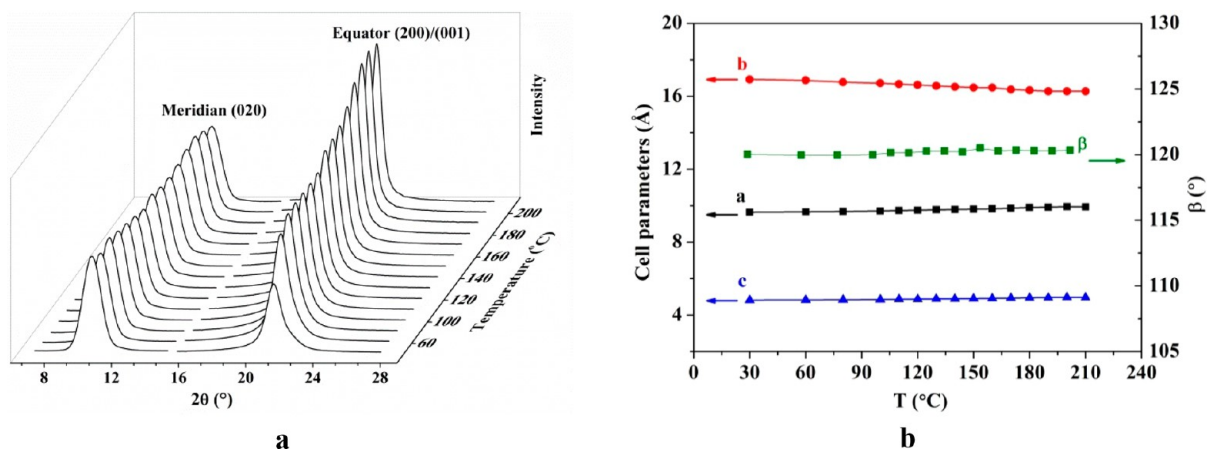


**Figure 5.** (a) 1D WAXD intensity profiles of the oriented  $\gamma$ -PA6 along the meridian and equator obtained at different temperatures. (b) Unit cell parameters of  $\gamma$ -PA6 as functions of temperature.

transition is associated with the enhanced librational motion of methylene sequence, while the hydrogen-bonded sheets are

maintained.<sup>37–40</sup> The “incomplete Brill transition” of  $\alpha$ -PA6 can be considered from this viewpoint. Namely, upon heating

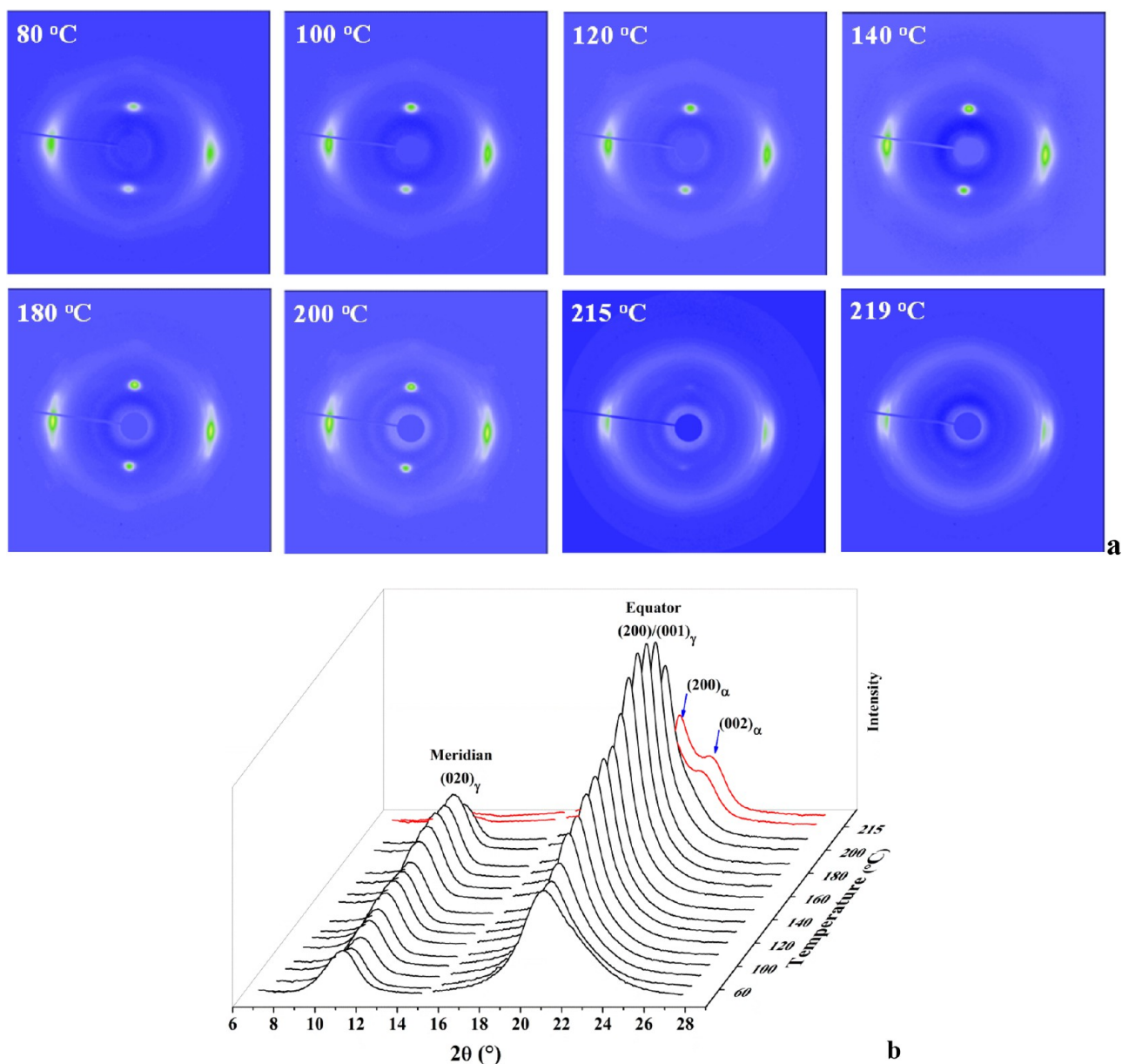


**Figure 6.** (a) 2D WAXD patterns of the oriented  $\beta$ -PA6 film at various temperatures recorded during heating; The meridian direction is parallel to the stretching direction. (b) 1D WAXD intensity profiles of the  $\beta$ -PA6 along the meridian and equator obtained at different temperatures.

more methylenes on the PA6 chains change their conformation from *trans* to *gauche*. This conformational change can be inferred from the small but detectable contraction of *b*-axis (chain axis).

In our experiment of  $\alpha$ -PA6, it is also observed that the diffractions of (200) and (002) separate slightly from each other instead of moving closer at 219 °C, just before the ultimate melting. This is likely related to the transformation of PA6 from  $\alpha$  to  $\alpha'$  form proposed by Murthy et al., which was often observed at around 170 °C for unoriented PA6 samples.<sup>27</sup> However, since it is unable to clearly recognize the diffractions other than (200) and (002), we failed to determine crystal lattice parameters at near the crystal melting.

Compared to  $\alpha$ -PA6, the phase transition behavior of  $\gamma$ -PA6 is simpler. Figure 5a shows the 1D intensity profiles of meridional ( $2\theta < 15^\circ$ ) and equatorial ( $2\theta > 15^\circ$ ) scans obtained from the 2D WAXD patterns (Figure S2) for different temperatures. During heating, the single diffraction peak on the

equator, i.e., the (200)/(001) diffraction, increases in intensity, becomes narrower, and moves slightly to the larger angle. This indicates that the  $\gamma$ -PA6 film obtained from KI/I<sub>2</sub> treatment of the oriented  $\beta$ -PA6 has a perfection process. The (200)/(001) diffraction is hard to be deconvoluted, implying the pseudo-hexagonal structure existing in the entire temperature range. Together with the (020) diffraction on the equator and other diffractions (e.g., (211) diffraction) observed in the quadrant, temperature-dependent unit cell parameters of the  $\gamma$ -PA6 can also be obtained. As shown in Figure 5b, variation of these parameters is little. Although metastable, the  $\gamma$ -form does not change into the more stable  $\alpha$ -form during heating. When heated up to 213 °C, the  $\gamma$ -PA6 sample melted, in consistent with results reported,<sup>28</sup> and no recrystallization leading to  $\alpha$ -form was observed.

**Crystal Structure Evolution of Stretched  $\beta$ -PA6 during Heating.** Evolution of structure and morphology of the stretched  $\beta$ -PA6 upon heating is the focus of this work. Shown

in Figure 6a are the synchrotron 2D WAXD patterns of the  $\beta$ -PA6 film measured at different temperatures before the sample was completely melted. At first glance, the main change of the diffraction pattern takes place at 215 °C. Before this temperature, the diffractions mainly appear on the meridian (stretching direction) and the equator. At 215 °C or above, the meridional diffraction becomes very weak, and the previous single equatorial diffraction splits into two. The main diffractions locating on equator and meridian demonstrate that the orientation of  $\beta$ -PA6 is well preserved during heating. Figure 6b presents the 1D intensity profiles along the meridian ( $2\theta < 15^\circ$ ) and the equator ( $2\theta > 15^\circ$ ) obtained from the 2D WAXD of the  $\beta$ -PA6 film at different temperatures, which captures the main change of diffraction behavior more quantitatively. Careful examination of the 2D WAXD patterns can reveal that some faint diffractions emerge in the quadrants at  $\sim 120$  °C, which become clearer when the temperature becomes higher than 140 °C. Aforementioned, one can distinguish the crystalline phase and the mesophase of the oriented PA6 based on whether or not the quadrant diffractions, i.e., the  $(hkl)$  diffractions with  $k \neq 0$ , are observed. Therefore, the appearance of quadrant diffractions at  $\sim 120$  °C suggests the crystalline phase starting to develop in the oriented  $\beta$ -PA6 sample.

We estimated the crystallinity of  $\beta$ -PA6 film as a function of temperature. Worthy to mention is that the diffraction of  $\beta$ -form is hard to be separated from the true crystalline diffraction. Therefore, the crystallinity calculated from the 2D WAXD pattern contains the contribution of the  $\beta$ -form and thus is an apparent one, particularly for that of low temperatures. As shown in Figure 7, the apparent crystallinity

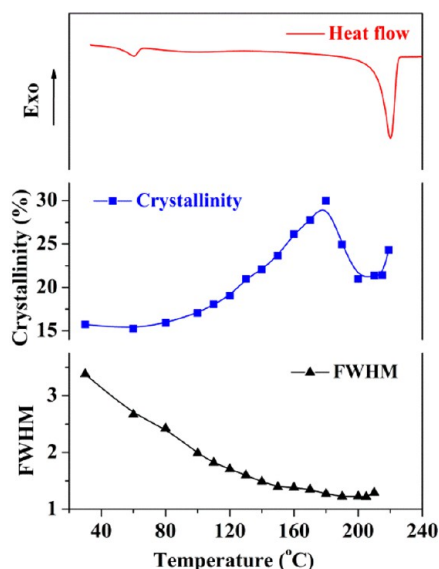


**Figure 7.** Apparent crystallinity and full width at half-height (fwhm) of the single equatorial diffraction of  $\beta$ -PA6 as functions of temperature. The DSC curve (red line) of  $\beta$ -PA6 is also plotted for comparison.

presents the change of “increase–decrease–increase” as the temperature rises. Namely, it monotonically increases up to 180 °C and then decreases until 210 °C followed by a slight increase. The first increase and the decrease of crystallinity are in consistent with the DSC heating result. The increase in crystallinity corresponds to the wide exothermic process occurring above the  $T_g$  of PA6, while the decrease after 180

°C is related to the endothermic process of melting. Since stayed at each temperature for 8 min, the sample was actually subjected to a stepwise annealing process. This causes the temperature at which the crystallinity drops to be higher than the beginning temperature ( $\sim 160$  °C) of the endotherm revealed by DSC. The second increase in crystallinity is associated with a recrystallization process, which is not reflected in the DSC experiment.

We consider that the first increase of crystallinity shall mainly correspond to the transformation from  $\beta$ - to  $\gamma$ -form. The 2D WAXD patterns of the  $\beta$ -PA6 film recorded at below 215 °C (Figure 6) look quite similar to that shown in Figure S2 of the  $\gamma$ -PA6. For these two samples, strong diffractions can be observed on the equator and the meridian. Figure 6b shows that the 1D WAXD profiles at below 215 °C are indeed reminiscent of that for the  $\gamma$ -PA6 (Figure 5a). To show the comparison more quantitatively, in Figure 8 we plot together some equatorial and meridional diffraction scans for the oriented  $\beta$ -,  $\gamma$ -, and  $\alpha$ -PA6 measured at same temperatures. As mentioned, the equatorial diffraction of the original  $\beta$ -PA6 film is obviously wider than the (200)/(001) diffraction of  $\gamma$ -PA6 (Figure 1c). It continuously narrows with increasing temperature. Albeit a little bit wider, it peaks at the almost same position as that of  $\gamma$ -PA6 at temperatures ranging from 180 to 210 °C (Figure 8a). For the meridional diffraction (Figure 8b), the peak of  $\beta$ -PA6 shifts to the left with increasing temperature and becomes identical to that of  $\gamma$ -PA6 at 200 °C. This outcome specifies that the thermal transition of  $\beta$ -PA6 can lead to the  $\gamma$ -PA6 crystals.

The formation of  $\gamma$ -PA6 crystals in the  $\beta$ -PA6 sample upon heating shall be based on a reorganization process. The continuous intensity enhancement of the single meridional diffraction until 180 °C and the monotonic decrease of full width at half-height (fwhh) of Figure 7 provide the evidence. Thermal FTIR result (Figure S3) indicated that the amount of free NH group was dramatically reduced when the temperature passed the  $T_g$  of PA6, indicating that more hydrogen bonds were formed once the PA6 chains became more mobile. As the chains are preoriented, rearrangement of the amide groups can construct the hydrogen bonding between the parallel chains that the  $\gamma$ -form requires.

The dramatic change of 2D WAXD of the  $\beta$ -PA6 samples occurs at 215 °C. Note that the melting temperature ( $T_m$ ) of  $\gamma$ -PA6 is of 213 °C. Therefore, the decrease of crystallinity shown in Figure 7 corresponds to the melting of  $\gamma$ -PA6. On the other hand, the second crystallinity increase shall be associated with the growth of  $\alpha$ -PA6 crystals. As shown in Figure 8, the (002) diffraction of  $\alpha$ -PA6 can hardly be recognized below 210 °C. However, it suddenly shows up at 215 °C, suggesting that the  $\alpha$ -PA6 crystallized rapidly even if the undercooling was very small. For the  $\gamma$ -PA6 film, no crystallization toward  $\alpha$ -PA6 is detected after the  $\gamma$ -PA6 is melted. Therefore, we suspect that some tiny crystals of  $\alpha$ -form may form during heating of the  $\beta$ -PA6, which can act as the seeds to promote the growth of  $\alpha$ -PA6. It is worth mentioning that the equatorial diffraction of the  $\beta$ -PA6 sample is constantly wider than that of  $\gamma$ -PA6 (Figure 8). Therefore, there may exist the (200) diffraction of  $\alpha$ -PA6 on the left side of the peak, as pointed by the arrows in Figure 8. This (200) diffraction shall be very weak, and thus the amount and the size of  $\alpha$ -PA6 crystals are small. At 210 °C, the right side of the equatorial diffraction of the  $\beta$ -PA6 sample is significantly increased, which can be partly due to the emergence of (002) diffraction of  $\alpha$ -PA6. Further increasing

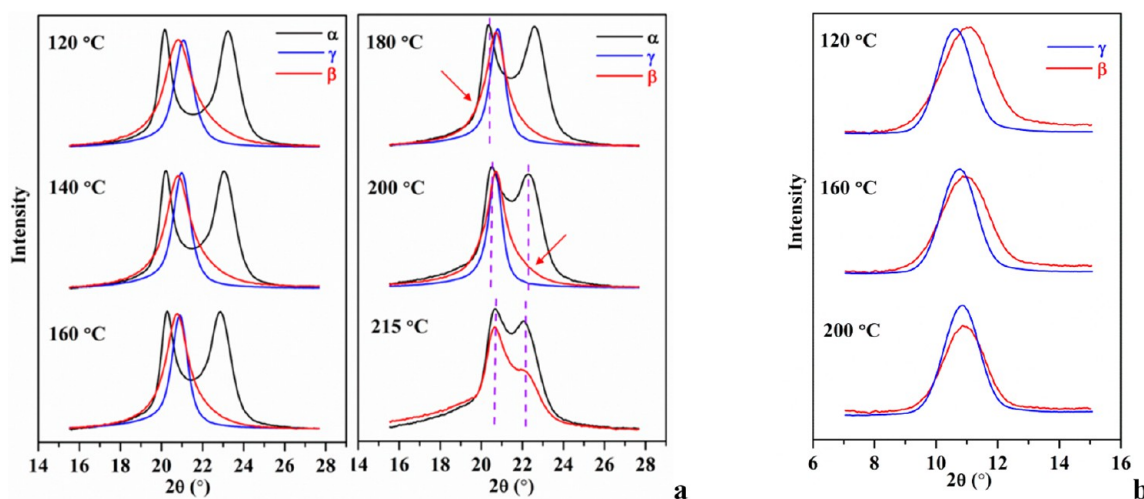


**Figure 8.** Comparison of the equatorial (a) and meridional (b) diffractions of the oriented  $\beta$ -,  $\gamma$ -, and  $\alpha$ -PA6 measured at different temperatures. The dashed purple lines indicates the positions of (200) and (002) diffractions of the  $\alpha$ -PA6. The arrows indicate the possible  $\alpha$ -form diffractions existing in the heated  $\beta$ -PA6 film.

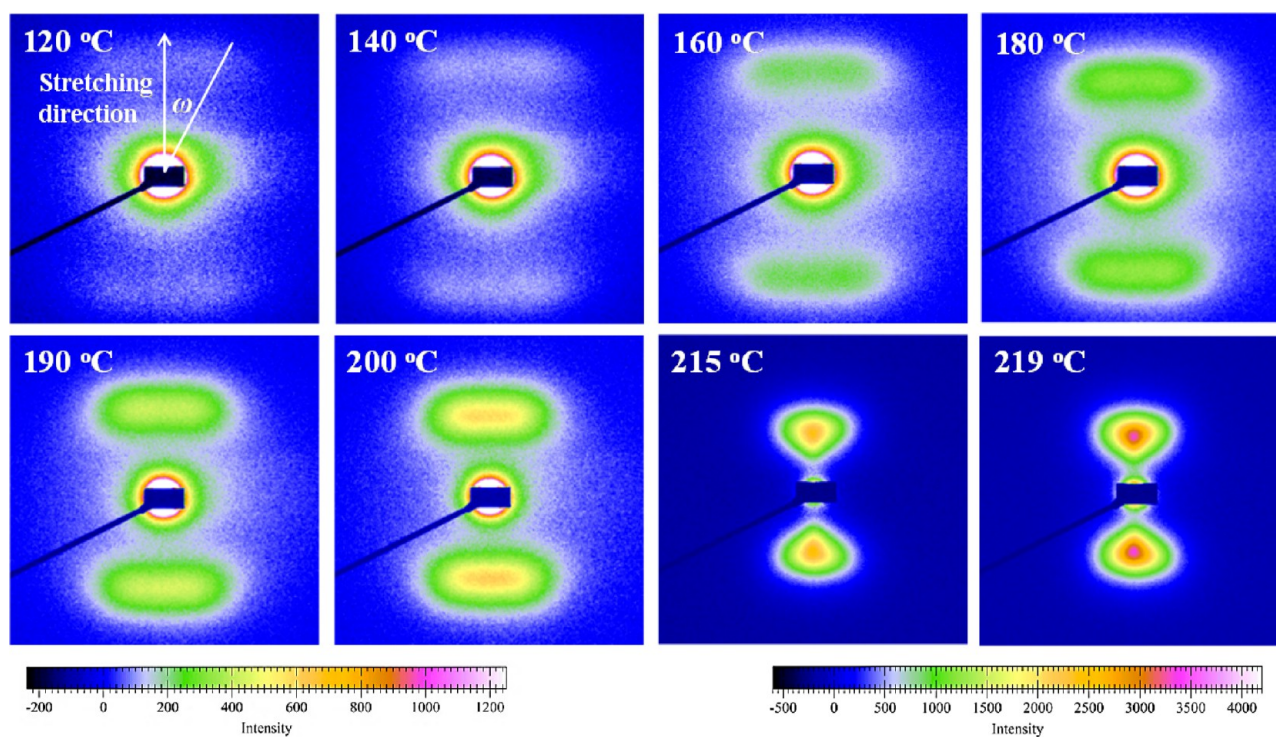


**Figure 9.** 2D SAXS patterns of the stretched  $\beta$ -PA6 film at various temperatures recorded during heating. The stretching direction is indexed by the arrow. The angle  $\omega$  is used to measure the range of lamellar tilting. The left intensity scale bar corresponds to the patterns below 215 °C, and the right intensity scale bar is for the patterns at 215 and 219 °C.

the temperature to crossover the melting of the  $\gamma$ -PA6 crystal, typical (200) and (002) diffractions of the  $\alpha$ -PA6 become clear.

**Crystal Morphology Evolution of Stretched  $\beta$ -PA6 during Heating.** The thermal transition from mesophase to crystalline phase of the stretched  $\beta$ -PA6 will certainly induce the change of crystal morphology. We carried out temperature-dependent SAXS experiments to follow the morphology evolution, of which some 2D patterns are shown in Figure 9. As mentioned earlier, there is no lamellar scattering of the stretched  $\beta$ -PA6 film at room temperature, which is an important feature for the mesophase. When the temperature rises up to 120 °C, diffuse and weak scattering appear at around

the  $q$  of  $\sim 1.03 \text{ nm}^{-1}$ , corresponding to a size of  $\sim 6 \text{ nm}$ . This dimension is fairly the segment length of 7 repeating units, 3 or 4 of which will later on pack into the crystal lattice. According to the WAXD result shown in Figure 7, the apparent crystallinity starts to increase right after the  $T_g$  of PA6 at around 60 °C, accompanied by the continuous narrowing of the equatorial diffraction of the  $\beta$ -PA6 sample. However, only when the temperature becomes as high as 120 °C can the small angle scattering and the wide-angle diffraction in quadrant be recognized. This implies that the chain reorganization takes time to result in the crystalline lamellae. Moreover, the first appearing small-angle scattering is so diffusive that it just

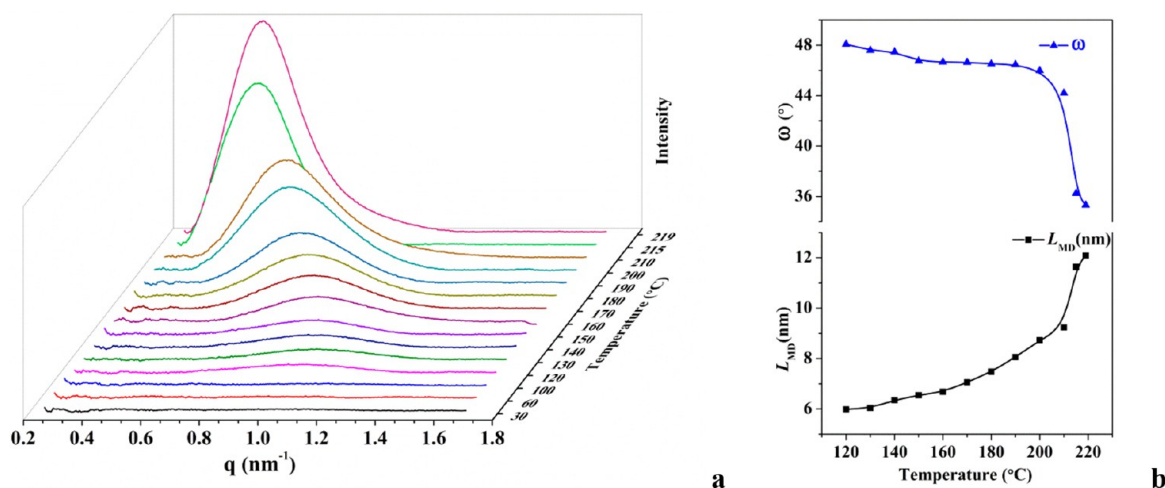


**Figure 10.** (a) Plots of SAXS intensity vs  $q$  measured for the oriented  $\beta$ -PA6 at various temperatures. (b) Long period corresponding to the meridional scattering ( $L_{MD}$ ) and lamellar tilting angle  $\omega$  (see Figure 9) as functions of temperature.

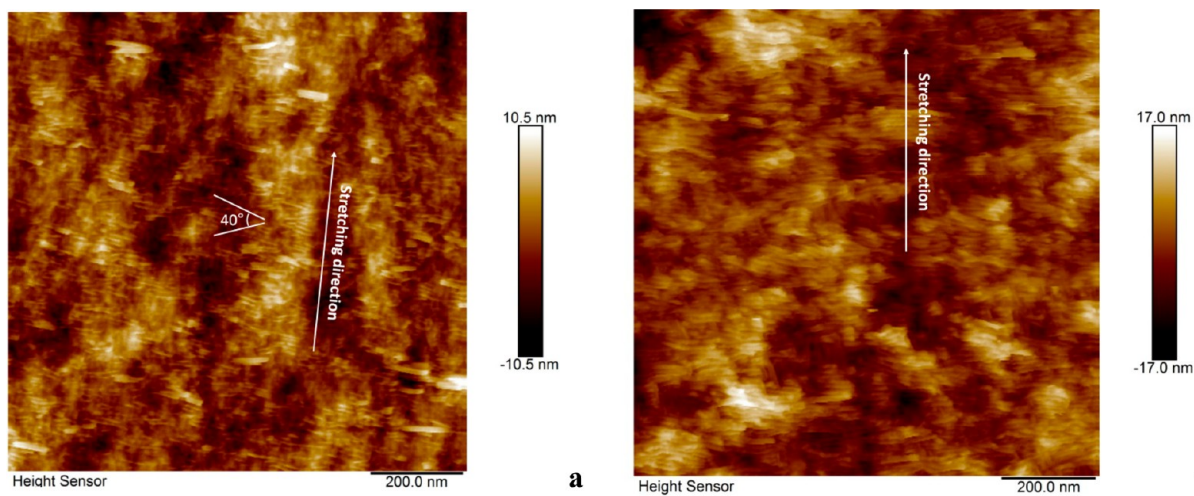


**Figure 11.** AFM images of the stretched PA6 films after annealing at (a) 200 °C and (b) 219 °C for 30 min. The arrows indicate roughly the stretching direction.

reflects an enhanced density fluctuation. After 120 °C the small-angle scattering becomes a meridional diffuse band. This band comes from the lamellar scattering. Moreover, it indicates that the lamellae have a distribution of orientation, wherein the lamellar basal surfaces are either perpendicular or tilted with respect to the stretching direction.

The meridional band scattering of the  $\beta$ -PA6 sample gradually increases in intensity and shifted to the lower angle until the scattering drastically changes to a two-point pattern at 215 °C. Figure 10a shows the plot of the scattering intensity vs  $q$  measured at various temperatures. For the lamellae giving the meridional band pattern, the long period corresponding to the scattering on meridional ( $L_{MD}$ ) is important, which indicates how long the segment of the oriented chain involved in the formation of lamellae. On the other hand, the angle  $\omega$  between the meridian and the scattering vector of the band tip (see Figure 9) can be used to measure the range of the lamellae tilting. Figure 10b describes a gentle increase of  $L_{MD}$  before 180 °C, while the  $\omega$  angle exhibits a slight decrease. Note that in this temperature range the crystallinity increases. Therefore, the lamellae are slightly thickened upon heating. The scattering intensity,  $L_{MD}$ , and  $\omega$  change more pronounced after 180 °C, in accordance with the decrease of crystallinity caused by the

melting of  $\gamma$ -PA6 (Figure 7). The reduction of  $\omega$  implies that the lamellae with larger tilting angle and smaller lamellar thickness undergo melting. The melting process enlarges the electron density difference between the crystalline and disorder region, leading to the stronger scattering at high temperatures.

After the  $\gamma$ -PA6 is melted, a drastic increase of scattering intensity and a sudden jump of the  $L_{MD}$  are observed. More importantly, the scattering changes to a two-point pattern, which indicates that the lamellar basal surface normal is mainly parallel to the stretching direction. It has been reported that for the  $\alpha$ -PA6 single crystal lamellae the chain stem is perpendicular to the fold surface.<sup>41</sup> Therefore, the two-point pattern represents the feature of the  $\alpha$ -form lamellae with the chain axis along the stretching direction.

The morphologies suggested by SAXS result can be confirmed by AFM results (Figure 11). The AFM samples were prepared by heating to a high temperature followed by 30 min annealing. From Figure 11a of the 200 °C annealed sample, the traces of fibrils caused by uniaxial stretching can be seen, which suggest that the stretching direction is nearly vertical. On the fibrils the lamellar stack is clear, of which the long period is around 7–8 nm, in fair agreement with that detected by SAXS at 200 °C. From stack to stack the lamellae

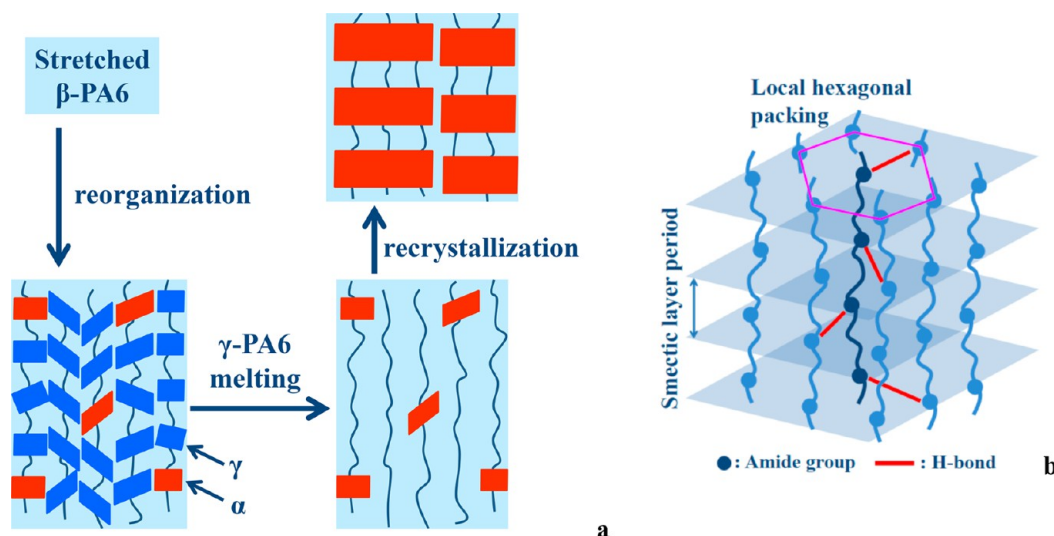


**Figure 12.** (a) Schematic diagram of the thermal transition pathway of the oriented  $\beta$ -PA6. (b) The  $\beta$ -form can be viewed as a smectic B-like structure. The smectic layer is composed of sublayers of amide group and methylene sequence. The dark blue chain in (b) is used as an example to show that the hydrogen bonds are randomly distributed around the chain axis.

can change the orientation more or less, resulting in an orientation distribution that reflected by the meridional band scattering. Indicated by the two white lines, an angle of  $\sim 40^\circ$  can be found between two lamellae. For the  $219^\circ\text{C}$  annealed sample, thicker lamellae can be observed (Figure 11b), which has the long period of 12–13 nm. Many lamellae align parallel to each other to form the stacks, and the orientation just has a narrow distribution. Moreover, the lateral size of the lamellae, which can exceed 200 nm, is much larger than that of  $\sim 30$  nm shown in Figure 11a. Clearly, this morphology can give the two-point SAXS pattern.

## DISCUSSION

On the basis of the temperature-dependent X-ray experiments, we have revealed the thermal transition pathway of the uniaxially stretched  $\beta$ -PA6. As shown by the schematic drawings in Figure 12a, upon heating, the  $\beta$ -PA6 will transform mainly to the  $\gamma$ -PA6 at first via reorganization, while some tiny  $\alpha$ -PA6 crystals also form. The resultant lamellae have a distribution of the basal surface normal, giving the meridional band scattering. A melt crystallization process will take place later on when the temperature crosses over the  $T_m$  of  $\gamma$ -PA6, resulting in the  $\alpha$ -PA6 lamellae with basal surface perpendicular to the stretch direction.

Our experiments demonstrate that the  $\beta$ -to- $\gamma$  transformation is the dominant process occurring first during heating, which is somewhat unexpected and conflicting with those reported in the literature.<sup>20,22</sup> To better rationalize this, we should go back to the chain packing in the  $\beta$ -form. As mentioned, the  $\beta$ -PA6 studied in this paper was produced by uniaxial stretching, giving the typical  $\beta$ -form diffraction pattern with the absence of the off-axes diffraction.<sup>18,21</sup> Without stretching, the PA6 films we had by melt quenching was amorphous with the halo center located at 0.413 nm. Therefore, the film stretching had greatly promoted the interchain hydrogen bonds once the chains were aligned parallel to each other. As under the stretching condition the PA6 chains are unable to adjust the conformation freely, a random distribution of hydrogen-bond directions is expected.<sup>18,21</sup> This causes the stretched  $\beta$ -PA6 film mesomorphic.

While the stretched  $\beta$ -PA6 film shares the same diffraction characteristics with the  $\beta$ -PA6 fibers produced by high-speed melt spinning,<sup>18,21</sup> i.e., only the equatorial and meridional diffraction are observed, careful examination reveals that their chain packing behaviors are somewhat different. As shown in Figure 1c, the equatorial diffraction of the stretched  $\beta$ -PA6 film is asymmetric. Peak deconvolution showed that using the combination of amorphous scattering and crystal diffraction (either  $\alpha$ ,  $\gamma$ , or  $\alpha$  and  $\gamma$ ) could not fit the asymmetric peak in satisfaction (Figure S4). However, it can be separated into one peak at 0.427 nm and an amorphous halo centered at 0.413 nm (Figure S5). Note that the  $d$ -spacing of 0.427 nm is larger than that of (100) diffraction (0.415 nm) of the melt spun  $\beta$ -PA6 fiber,<sup>21</sup> implying that the possible hexagonal packing is not very compact. Moreover, although the chains are well orientated, the amorphous scattering indicates that many chains in the film possess a short-range order laterally. This observation is in consistent with that the hydrogen bonds are not fully formed in the stretched  $\beta$ -PA6 film (Figure S3). On the other hand, we note that the meridional diffraction of our  $\beta$ -PA6 film gives the  $d$ -spacing is even smaller than that of the  $\beta$ -PA6 fiber (0.80 nm vs 0.83 nm), suggesting that the chains are more conformational disordered. As shown by the ATR-FTIR result (Figure S6) of the  $\beta$ -PA6 film, the conformation disorders exist in both the methylene sequences and the  $-\text{CH}_2\text{---C(=O)-}$  bonds.

We suggest that the  $\beta$ -form of the stretched PA6 film can be viewed as a solid mesophase with SmB-like structure. It has been suggested that nylon-11 adopts a smectic structure as its mesophase.<sup>42</sup> The stretched  $\beta$ -PA6 film is less ordered than the  $\beta$ -PA6 fiber reported.<sup>18,21</sup> As shown in Figure 12b, with the conformational disordered PA6 chains aligned parallel to each other, the smectic layer is composed of the amide sublayers and the methylene sublayer, which can provide the strong meridional diffraction along the stretching direction. The equatorial diffraction peak that observed after the peak deconvolution suggests a sort of local hexagonal packing of chains. Within the amide sublayer, the interchain hydrogen bonds can be partly formed. Since the stretched chains pass through different smectic layers, a hydrogen-bonded network is generated, which in fact helps to fix the chain orientation. We

consider that the hydrogen-bonded network of the oriented PA6 chains is very important.

For this mesomorphic  $\beta$ -PA6 film, using the meridional diffraction shown in 2D WAXD pattern (see Figure 1), we calculated the Hermans–Stein orientation distribution function ( $f_{MD}$ ):

$$f_{MD} = \frac{3\langle \cos^2 \phi_{MD} \rangle - 1}{2}$$

$$\langle \cos^2 \phi_{MD} \rangle = \frac{\int_0^{\pi/2} I(\phi) \sin \phi \cos^2 \phi \, d\phi}{\int_0^{\pi/2} I(\phi) \sin \phi \, d\phi}$$

where  $\phi$  is the azimuthal angle of the meridional diffraction and  $I$  the intensity.<sup>43</sup> For the chain completely oriented along the stretching direction,  $f_{MD} = 1$ , while for the fully random orientation  $f_{MD} = 0$ . The value of  $f_{MD}$  is estimated to be 0.53, manifesting a quite high degree of orientation. This chain orientation is robust. Note that the oriented samples of  $\alpha$ - and  $\gamma$ -PA6 examined in this study were prepared by annealing at 219 °C and KI/I<sub>2</sub> treatment, respectively, using the stretched  $\beta$ -PA6 as the precursor. For these two samples, the values of orientation distribution function  $f_{020}$  based on the (020) diffractions on the meridian are estimated to be of 0.67 and 0.82, respectively. As the two  $f_{020}$  functions mainly counts the orientation of chains in crystal, they are even higher than the  $f_{MD}$  for the mesomorphic  $\beta$ -PA6. This outcome reflects that under rigorous condition the original chain orientation can survive. We think that, at least, this shall be partly attributed to the network built up by the abundant hydrogen bond pairs in the stretched  $\beta$ -PA6. The hydrogen-bonded network is a dynamic system where hydrogen bonds are broken and formed all the time. Nevertheless, this dynamic process will not cause a catastrophe of the network before the film is completely melted or dissolved.

It is known that rapid cooling or melt spinning can facilitate the growth of PA6 crystals of  $\gamma$ -form.<sup>44</sup> Differently, in our study, the  $\gamma$ -PA6 crystals are formed during heating and in a quiescent state. In this case, we presume that a confinement effect arises from the hydrogen-bonded network of oriented chains plays a critical role. Paul et al. found that in PA6/montmorillonite composites the crystallization of  $\gamma$ -PA6 was greatly enhanced.<sup>45</sup> They suggest that the interaction between PA6 chains and the nanoclay can provide a confinement effect, and thus the chains with reduced mobility can pack into  $\gamma$ -PA6 more readily. In our investigation of thin film crystallization of PA6, we observed that on the mica substrate covered by a thin layer of carbon the PA6 film with thickness less than 50 nm could grow the flat-on  $\gamma$ -PA6 lamellae, which also reflects the confinement effect.<sup>46</sup> For the stretched  $\beta$ -PA6 film studied here, the  $\gamma$ -PA6 crystals are formed through the reorganization between the chains. Local melting of the pseudohexagonal domains can happen gradually during heating, letting some hydrogen bonds to dissociate and thus to allow the rearrangement of amide groups. Meanwhile, other hydrogen bonds substantially restrict the chain mobility. Under this condition, the formation of  $\gamma$ -PA6 becomes favorable. Moreover, as the mesomorphic  $\beta$ -form has the lateral chain packing more similar to the pseudohexagonal  $\gamma$ -form than the  $\alpha$ -form, this may also be helpful to the easy conversion from  $\beta$ - to  $\gamma$ -form.

To further confirm that the  $\beta$ -to- $\gamma$  transformation can happen in the stretched  $\beta$ -PA6 with the hydrogen-bonded network

composed of oriented chains, we annealed the stretched  $\beta$ -PA6 films at different temperatures for 30 min and then cooled the samples to room temperature. The 1D WAXD profiles recorded at room temperature are summarized in Figure 13,

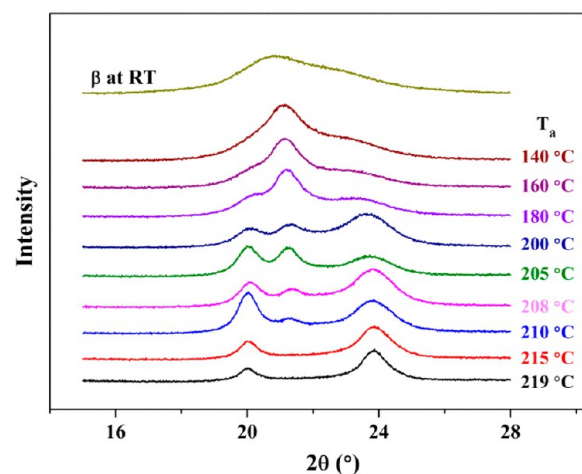


**Figure 13.** WAXD profiles of  $\beta$ -PA6 films recorded at room temperature after annealing at different temperatures ( $T_a$ s) for 30 min.

wherein the data of original  $\beta$ -PA6 film are included for comparison. For the annealing temperatures ( $T_a$ s) lower than 180 °C, the 1D WAXD profiles acquired at room temperature look like a combination of that of  $\gamma$ - and  $\beta$ -form. Increasing  $T_a$  leads to more pronounced diffraction of  $\gamma$ -PA6. For 180 °C  $\leq T_a < 215$  °C, the diffractions of  $\gamma$ - and  $\alpha$ -form superpose together. The higher the  $T_a$ , the stronger the  $\alpha$ -form diffraction is. As shown in Figures 6 and 8, in the continuous heating experiment the  $\alpha$ -PA6 crystal is largely absent in this temperature range. Therefore, the significant amount of  $\alpha$ -PA6 in the annealed samples should be resulted from the cooling process where the normal crystallization of PA6 occurs. At 213 °C  $\leq T_a < 221$  °C, i.e., at the temperatures between the  $T_m$ s of  $\gamma$ - and  $\alpha$ -PA6, the pure  $\alpha$ -PA6 can be obtained.

It is found that the  $\alpha$ -PA6 developed at the  $T_a$  higher than the  $T_m$  of  $\gamma$ -PA6 still exhibits high orientation. For this case, one remark is that the small  $\alpha$ -form crystallites formed during heating may act as strong physical cross-links to retain the original hydrogen-bonded network. They can further serve as the nuclei for  $\alpha$ -PA6 crystallization (see Figure 12a). On the other hand, although relaxed partly, the oriented PA6 chains can crystallize faster than those in the isotropic undercooled melt. In fact, taking this advantage, we prepared the highly oriented  $\alpha$ -PA6 film, of which the morphology is shown in Figure 11b.

The meridional band scattering shown in Figure 9 can also be a consequence of the hydrogen-bonded network of oriented PA6 chains. The meridional band pattern is frequently observed for semicrystalline polymers subjected to stretching.<sup>47–51</sup> Upon stretching, the isotropic spherulites can be transformed to an anisotropic structure due to the chain orientation. Accordingly, the original isotropic small-angle scattering evolves into a meridional band pattern. It is interpreted that the band scattering perpendicular to the stretching direction comes from a composite of lamellar stacks shearing at different levels, which exhibits a distribution of lamellar basal surface angles.<sup>52</sup> For the  $\beta$ -PA6 sample studied, no external shear force was applied during the 2D SAXS measurement. Therefore, the meridional

band pattern, which reveals that the lamellar orientation has a distribution, shall be associated with the lamellae developed from the oriented chains.

We suppose that at the beginning the dynamic dissociation/association of the hydrogen-bonding interaction can cause the density fluctuation. As more hydrogen bonds formed to reduce the free energy of the sample, some dense domains emerge, leading to the diffusive scattering emerging at 120 °C. However, to achieve the lamellar morphology, the oriented chains need to adjust many times the amide group positions and the conformation of methylene sequences. Note that this process invokes chain segments with a few repeating units participating in the hydrogen-bonded network. Therefore, the chain adjustment is subjected to the network confinement. The same as other crystalline polymers, the oriented  $\beta$ -PA6 sample intends to increase the crystallinity as fast as possible. With the limited chain mobility, many of the oriented PA6 chains will no longer seek the way to form perfect lamellae. Once they pack into the crystalline lattice, the chain adjustment will stop. This process results in the lamellae with a relatively broad distribution of basal surface normal. The tilted lamellae in fact can reduce the possible overcrowding at the lamellar interface which can be caused by noncrystalline PA6 chain segments emanating from the lamellae.<sup>51</sup> In addition, the reorganization toward to crystals may cause some internal stress. Through the hydrogen-bonded network the stress may induce shear on the lamellae, resulting in the  $\omega$  angle of  $\sim 45^\circ$ .

As shown by Figure 10, the PA6 lamellae at above 210 °C possess the long period significantly larger than that at lower temperatures. A similar drastic increase of long period is observed for doubly oriented nylon-10,10 at near the  $T_m$  by Tashiro.<sup>26</sup> It is proposed that after the Brill transition of nylon-10,10 the chains without constrain of hydrogen bonds can possess the active translational motion along the chain axis, leading to the thicker lamellae. For the stretched PA6 sample studied here, after the  $\gamma$ -PA6 is melted, the dissociation of hydrogen bond shall also be quite active, weakening the confinement by the hydrogen-bonded network. The oriented chains can adjust more adequately so that the lamellae with the basal surface perpendicular to the chain axis can be achieved. Moreover, as shown in Figure 11, the  $\alpha$ -PA6 lamellae formed at 219 °C not only are thicker but also have much larger lateral dimension than that the lamellae formed after annealing at 200 °C.

## CONCLUSION

In summary, we have investigated the thermal transition of uniaxially stretched  $\beta$ -PA6 film, which was monitored mainly by means of temperature-dependent 2D WAXD and SAXS. The  $\beta$ -form in the stretched PA6 film, which can be viewed as a solid mesophase with SmB-like structure, has the layer structure composed of the amide group sublayer and the methylene sublayer, and within the layer a sort of local hexagonal packing exists. More importantly, the amide groups in their sublayers can form hydrogen bonds randomly, making a network that sustains chain orientation upon heating. To elucidate the transformation pathway of the  $\beta$ -PA6 during heating, we take the thermal 2D WAXD results of the orientated  $\alpha$ - and  $\gamma$ -PA6, which show an “incomplete Brill transition” for the  $\alpha$ -PA6 and the direct melting for the  $\gamma$ -PA6, respectively, as the references. The detailed comparisons reveal that the stretched  $\beta$ -PA6 will mainly reorganize into the  $\gamma$ -PA6 via the rearrangement of the hydrogen bonds. Meanwhile, a little amount of small  $\alpha$ -PA6

crystals forms, which can help to retain the hydrogen-bonded network and accelerate the subsequent melt crystallization of the  $\alpha$ -PA6. The 2D SAXS experiment indicates that no lamellar scattering can be detected in the original stretched  $\beta$ -PA6 sample. The lamellar scattering appears after the  $\gamma$ -form WAXD pattern can be recognized. The meridional band scattering pattern suggests that the lamellae have a distribution of basal surface orientation. Once the crystallization occurs after the melting of  $\gamma$ -PA6 lamellae, a two-point scattering pattern is observed, indicating that the newly formed  $\alpha$ -PA6 lamellae possess the basal surface perpendicular to the stretching direction. For the thermal transition of the stretched  $\beta$ -PA6, we consider that the hydrogen-bonded network of the oriented chains plays the critical role. The confinement effect arising from the network reduces the chain mobility, favoring the  $\beta$ -to- $\gamma$  transition. Also, this effect causes the appearance of tilted lamellae which are less perfect. Our work provides new insights into the structure and transition of  $\beta$ -PA6. In industry, large amounts of PA6 films are produced by melt quenching and stretching. For this matter, the results reported here are important for the control of the structures and properties of PA6 films. Furthermore, we anticipate that the results can also be used for exploring new applications of PA6 materials.

## ASSOCIATED CONTENT

### Supporting Information

The Supporting Information is available free of charge on the ACS Publications website at DOI: 10.1021/acs.macromol.7b01827.

2D WAXD pattern of the quenched PA6 film without stretching; 2D WAXD patterns of the oriented  $\gamma$ -PA6 films recorded at different temperatures; FTIR results of the stretched  $\beta$ -PA6 film; peak deconvolution of the equatorial diffraction of the stretched  $\beta$ -PA6; ATR-FTIR spectra of  $\beta$ -PA6 and  $\alpha$ -PA6 at room temperature (PDF)

## AUTHOR INFORMATION

### Corresponding Authors

\*E-mail: eqchen@pku.edu.cn (E.Q.C.).

\*E-mail: Alexander.Stroeks@dsm.com (A.S.).

### ORCID

Xiang-Kui Ren: 0000-0001-7894-9361

Er-Qiang Chen: 0000-0002-0408-5326

### Notes

The authors declare no competing financial interest.

## ACKNOWLEDGMENTS

The work at PKU was sponsored by DSM Research and the National Natural Science Foundation of China (Grant No. 21474002). The authors thank Dr. Y. B. Huang (DSM Research) for fruitful discussions. For X-ray experiments, the help from Dr. Guang Mo at the Beijing Synchrotron Radiation Facility (SSRF) and Dr. W. S. Bu at Institute of Chemistry, CAS, is greatly appreciated.

## REFERENCES

- (1) Kohan, M. I. *Nylon Plastics Handbook*; Carl Hanser Verlag: 1995.
- (2) Kotek, R.; Jung, D.; Tonelli, A. E.; Vasanthan, N. Novel methods for obtaining high modulus aliphatic polyamide fibers. *J. Macromol. Sci., Polym. Rev.* **2005**, *45*, 201–230.
- (3) Haines, C. S.; Lima, M. D.; Li, N.; Spinks, G. M.; Foroughi, J.; Madden, J. D. W.; Kim, S. H.; Fang, S.; Jung de Andrade, M.; Göktepe,

- F.; Göktepe, Ö.; Mirvakili, S. M.; Naficy, S.; Lepró, X.; Oh, J.; Kozlov, M. E.; Kim, S. J.; Xu, X.; Swedlove, B. J.; Wallace, G. G.; Baughman, R. H. Artificial Muscles from Fishing Line and Sewing Thread. *Science* **2014**, *343* (6143), 868–872.
- (4) Kinoshita, Y. An Investigation of the Structure of Polyamide Series. *Makromol. Chem.* **1959**, *33*, 1–20.
- (5) Atkins, E. D. T.; Hill, M.; Hong, S. K.; Keller, A.; Organ, S. Lamellar Structure and Morphology of Nylon 46 crystals: A New Chain Folding Mechanism for Nylons. *Macromolecules* **1992**, *25*, 917–924.
- (6) Zhang, G.; Yan, D. Morphology and Structure of Chain-Folded Lamellar Crystals of Nylons 2 22, 4 22, 6 22, 8 22, 10 22, and 12 22. *Cryst. Growth Des.* **2004**, *4* (2), 383–387.
- (7) Murthy, N. S. Hydrogen bonding, Mobility, and Structural Transitions in Aliphatic Polyamides. *J. Polym. Sci., Part B: Polym. Phys.* **2006**, *44* (13), 1763–1782.
- (8) Holmes, D. R.; Bunn, C. W.; Smith, D. J. The Crystal Structure of Polycaprolactone - Nylon-6. *J. Polym. Sci.* **1955**, *17* (83), 159–177.
- (9) Murthy, N. S.; Aharoni, S. M.; Szollosi, A. B. Stability of the  $\gamma$  Form and the Development of the  $\alpha$  Form in Nylon 6. *J. Polym. Sci., Polym. Phys. Ed.* **1985**, *23* (12), 2549–2565.
- (10) Murthy, N. S.; Bray, R. G.; Correale, S. T.; Moore, R. A. F. Drawing and Annealing of Nylon-6 Fibres: Studies of Crystal Growth, Orientation of Amorphous and Crystalline Domains and Their Influence on Properties. *Polymer* **1995**, *36* (20), 3863–3873.
- (11) Liu, Y.; Cui, L.; Guan, F.; Gao, Y.; Hedin, N. E.; Zhu, L.; Fong, H. Crystalline Morphology and Polymorphic Phase Transitions in Electrospun Nylon-6 Nanofibers. *Macromolecules* **2007**, *40* (17), 6283–6290.
- (12) Liu, X.; Wu, Q. Phase Transition in Nylon 6/Clay Nanocomposites on Annealing. *Polymer* **2002**, *43* (6), 1933–1936.
- (13) Arimoto, H.; Ishibashi, M.; Hirai, M.; Chatani, Y. Crystal Structure of the Gamma-Form of Nylon 6. *J. Polym. Sci., Part A: Gen. Pap.* **1965**, *3*, 317–326.
- (14) Kyotani, M.; Mitsuhashi, S. Studies on crystalline forms of nylon 6. II. Crystallization From the Melt. *J. Polym. Sci., Part A-2: Polym. Phys.* **1972**, *10* (8), 1497–1508.
- (15) Cavallo, D.; Gardella, L.; Alfonso, G. C.; Portale, G.; Balzano, L.; Androsch, R. Effect of Cooling Rate on the Crystal/mesophase Polymorphism of Polyamide 6. *Colloid Polym. Sci.* **2011**, *289*, 1073–1079.
- (16) Arimoto, H.  $\alpha$ - $\gamma$  Transition of nylon 6. *J. Polym. Sci., Part A: Gen. Pap.* **1964**, *2* (5), 2283–2295.
- (17) Abuisa, I. Alpha-Gamma Transition in Nylon-6. *J. Polym. Sci., Part A-1: Polym. Chem.* **1971**, *9* (1), 199–216.
- (18) Ziabicki, A. Über die mesomorphe  $\beta$ -Form von Polycapronamid und ihre Umwandlung in die kristalline Form  $\alpha$ . *Colloid Polym. Sci.* **1959**, *167* (2), 132–141.
- (19) Mileva, D.; Androsch, R.; Zhuravlev, E.; Schick, C. Morphology of Mesophase and Crystals of Polyamide 6 Prepared in a Fast Scanning Chip Calorimeter. *Polymer* **2012**, *53* (18), 3994–4001.
- (20) Penel-Pierron, L.; Depecker, C.; Séguéla, R.; Lefebvre, J. M. Structural and Mechanical Behavior of Nylon 6 Films Part I. Identification and Stability of the Crystalline Phases. *J. Polym. Sci., Part B: Polym. Phys.* **2001**, *39* (5), 484–495.
- (21) Auriemma, F.; Petraccone, V.; Parravicini, L.; Corradini, P. Mesomorphic Form ( $\beta$ ) of Nylon 6. *Macromolecules* **1997**, *30* (24), 7554–7559.
- (22) Stepaniak, R. F.; Garton, A.; Carlsson, D. J.; Wiles, D. M. An Examination of the Crystal Structures Present in Nylon-6 Fibers. *J. Polym. Sci., Polym. Phys. Ed.* **1979**, *17* (6), 987–999.
- (23) Murthy, N. S. Metastable Crystalline Phases in Nylon 6. *Polym. Comm.* **1991**, *32* (10), 301–305.
- (24) Androsch, R.; Stolp, M.; Radsch, H. J. Crystallization of Amorphous Polyamides From the Glassy State. *Acta Polym.* **1996**, *47*, 99–104.
- (25) Pepin, J.; Miri, V.; Lefebvre, J.-M. New Insights into the Brill Transition in Polyamide 11 and Polyamide 6. *Macromolecules* **2016**, *49*, 564–573.
- (26) Tashiro, K. Structural Phase Transition of Aliphatic Nylons Viewed from the WAXD/SAXS and Vibrational Spectral Measurements and Molecular Dynamics Calculation. *Chin. J. Polym. Sci.* **2007**, *25*, 73–82.
- (27) Murthy, N. S.; Curran, S. A.; Aharoni, S. M.; Minor, H. Premelting Crystalline Relaxations and Phase Transitions in Nylon 6 and 6,6. *Macromolecules* **1991**, *24*, 3215–3220.
- (28) Ramesh, C.; Gowd, E. B. High-Temperature X-ray Diffraction Studies on the Crystalline Transitions in the  $\alpha$ - and  $\gamma$ -Forms of Nylon-6. *Macromolecules* **2001**, *34*, 3308–3313.
- (29) Lincoln, D. M.; Vaia, R. A.; Wang, Z.-G.; Hsiao, B. S.; Krishnamoorti, R. Temperature Dependence of Polymer Crystalline Morphology in Nylon 6/montmorillonite Nanocomposites. *Polymer* **2001**, *42*, 09975–09985.
- (30) Brill, R. Über das Verhalten von polyamiden beim Erhitzen. *J. Prakt. Chem.* **1942**, *161*, 49–64.
- (31) Hsiao, B. S.; Kennedy, A. D.; Leach, R. A.; Chu, B.; Harney, P. Studies of Structure and Morphology Development During the Heat-Draw Process of Nylon 66 Fiber by Synchrotron X-ray Diffraction and Scattering Techniques. *J. Appl. Crystallogr.* **1997**, *30*, 1084–1095.
- (32) Ramesh, C.; Keller, A.; Eltink, S. J. E. A. Studies on the Crystallization and Melting of Nylon-6,6:1. The Dependence of the Brill Transition on the Crystallization Temperature. *Polymer* **1994**, *35*, 2483–2487.
- (33) Vasanathan, N.; Murthy, N. S.; Bray, R. G. Investigation of Brill Transition in Nylon 6 and Nylon 6,6 by Infrared Spectroscopy. *Macromolecules* **1998**, *31*, 8433–8435.
- (34) Ramesh, C. New Crystalline Transitions in Nylons 4,6, 6,10, and 6,12 Using High Temperature X-ray Diffraction Studies. *Macromolecules* **1999**, *32*, 3721–3726.
- (35) Zhang, Q.; Mo, Z.; Zhang, H.; Liu, S.; Cheng, S. Z. D. Crystal Transitions of Nylon 11 Under Drawing and Annealing. *Polymer* **2001**, *42*, 5543–5547.
- (36) Cooper, S. J.; Coogan, M.; Everall, N.; Priestnall, I. A Polarised  $\mu$ -FTIR Study on a Model System for Nylon 6 6: Implications for the Nylon Brill structure. *Polymer* **2001**, *42*, 10119–10132.
- (37) Miura, H.; English, A. D. Segmental Dynamics in Nylon 66. *Macromolecules* **1988**, *21* (5), 1543–1544.
- (38) Hirschingner, J.; Miura, H.; Gardner, K. H.; English, A. D. Segmental Dynamics in the Crystalline Phase of Nylon 66. Solid-State 2H NMR. *Macromolecules* **1990**, *23* (8), 2153–2169.
- (39) Wendoloski, J. J.; Gardner, K. H.; Hirschingner, J.; Miura, H.; English, A. D. Molecular Dynamics in Ordered Structures: Computer Simulation and Experimental Results for Nylon 66 Crystals. *Science* **1990**, *247* (4941), 431–436.
- (40) Tashiro, K.; Yoshioka, Y. Molecular Dynamics Simulation of the Structural and Mechanical Property Changes in the Brill Transition of Nylon 10/10 Crystal. *Polymer* **2004**, *45* (12), 4337–4348.
- (41) Geil, P. H. Nylon Single Crystals. *J. Polym. Sci.* **1960**, *44* (144), 449–458.
- (42) Nair, S. S.; Ramesh, C.; Tashiro, K. Crystalline Phases in Nylon-11: Studies Using HTWAXS and HTFTIR. *Macromolecules* **2006**, *39*, 2841–2848.
- (43) Trottier, A. M.; Zwanziger, J. W.; Murthy, N. S. Amorphous orientation and its relationship to processing stages of blended polypropylene/polyethylene fibers. *J. Appl. Polym. Sci.* **2008**, *108* (6), 4047–4057.
- (44) Heuvel, H. M.; Huisman, R. Effects of Winding Speed, Drawing and Heating on the Crystalline Structure of Nylon 6 Yarns. *J. Appl. Polym. Sci.* **1981**, *26* (2), 713–732.
- (45) Fornes, T. D.; Paul, D. R. Crystallization Behavior of Nylon 6 Nanocomposites. *Polymer* **2003**, *44* (14), 3945–3961.
- (46) Zhong, L.-W.; Ren, X.-K.; Yang, S.; Chen, E.-Q.; Sun, C.-X.; Stroeks, A.; Yang, T.-Y. Lamellar Orientation of Polyamide 6 Thin Film Crystallization on Solid Substrates. *Polymer* **2014**, *55* (16), 4332–4340.
- (47) Bonart, R.; Hosemann, R. Fibrillarstrukturen in kaltverrecktem linearen Polyäthylen. *Colloid Polym. Sci.* **1962**, *186*, 16.

(48) Fronk, W.; Wilke, W. Two-dimensional Analysis of the SAXS of Partially Oriented Polymers. *Colloid Polym. Sci.* **1983**, *261* (12), 1010–1021.

(49) Lin, L.; Argon, A. S. Deformation Resistance in Oriented Nylon 6. *Macromolecules* **1992**, *25* (15), 4011–4024.

(50) Murthy, N. S.; Grubb, D. T.; Zero, K. Structural Implications of the Elliptical Form of Small-Angle Reflections in Oriented Semicrystalline Polymers. *Macromolecules* **2000**, *33* (3), 1012–1021.

(51) Murthy, N. S.; Grubb, D. T. Deformation of Lamellar Structures: Simultaneous Small- and Wide-angle X-ray Scattering Studies of Polyamide-6. *J. Polym. Sci., Part B: Polym. Phys.* **2002**, *40* (8), 691–705.

(52) Song, H. H.; Argon, A. S.; Cohen, R. E. Morphology of Highly Textured High-density Polyethylene. *Macromolecules* **1990**, *23* (3), 870–876.